EXPERIMENTAL AND NUMERICAL INVESTIGATION ON SINGLE AIR BUBBLE RISING IN NARROW RECTANGULAR CHANNEL

Liqin Zhang, Yanping Huang*, and Yuanfeng Zan, Junfeng Wang, Mingliang Song
CNNC Key Laboratory on Nuclear Reactor Thermal Hydraulics Technology
Nuclear Power Institute of China, Chengdu 610041, PR China
Liqinzhang001@163.com; hyanping007@163.com; yfzan@163.com; walojef@163.com;
Songmingliang1986@163.com

ABSTRACT

Flow regimes identification is the most key precondition for two phase flow and boiling heat transfer calculations. Recent research has shown that flow regimes of air-water two phase flow in narrow rectangular channel are different from that of vapor-water two phase flow. Investigations on single air bubble rising are of fundamental significance to disclosure differences between air-water and vapor-water two phase flow regimes. In this paper, motion characteristics of single air bubble rising in a vertical narrow rectangular channel are studied numerically and experimentally, and effects of inlet average fluid velocity on terminal rising velocity, bubble shape, wake structure and velocity profiles are analyzed. Air bubbles were produced by injecting air into the test section of $60 \times 2 \times 950$ mm^3, and bubbles with diameter of 2.0-24.5 mm rising through water with inlet average fluid velocities 0.0-0.2 m/s were examined by PIV. Numerical analysis employing Level Set model based on TransAT platform is carried out. Results showed that experimental and calculated terminal rising velocities were comparable. Increasing the inlet average fluid velocity led to deeper dimple appeared in bubble bottom and less disturbances in the wake. Wake with less disturbances is expected to be bad to bubble coalescence. Position achieved stable velocity ahead of bubble was about $0.75W$ from the bubble and not affected by inlet average fluid velocities. But Position with maximum velocity in the wake moved to bubble bottom as inlet average fluid velocity increased. Numerical data are consistent with experimental data, which indicates that Level Set model can be used to simulate single air bubble rising in narrow rectangular channel. Results attained can be input to analyzing bubble interaction which is closely related with flow regime transitions.

KEYWORDS
Air-water/vapor-water, two-phase flow, bubble motion, narrow rectangular channel, thermal hydraulics

1. INTRODUCTION

Due to its simpler construction and larger specific surface area, narrow rectangular channel has higher heat exchange efficiency being widely used in heat exchange systems with smaller volume and higher power density with many of them are vapor-water two-phase flow systems. In order to strengthen heat transfer, gap of the rectangular channel is always less than 3 mm belonging to narrow channel. Nowadays, flow pattern graph widely used are mainly obtained from air-water two phase flow. Available investigations show that flow patterns and its transition criterion of air-water two phase flow in the narrow rectangular channel are different from that of vapor-water two phase flow [1-3]. Studying and

* Corresponding author, E-mail: hyanping007@163.com

disclosuring its difference mechanism is of fundamental significance for using flow pattern graph correctly with investigating single bubble behaviour as a basic step.

According to channel gap as its character dimension, flow channels are divided into general channel (> 5 mm), narrow space or confined space (0.5-5 mm), microscale(0.01-0.5 mm or 0.01-1 mm) and capillary channel (< 0.01 mm). In the present study, gap of channel is 2 mm belonging to narrow space. Table 1 assembles publications dealing with single bubble movement in more or less confined geometries with rectangular cross sections, investigated with high speed cameras. The channel space is down to 1 mm (Roudet et al. (2007) [9]). The varied parameters are in most cases geometrical properties, bubble size (ranging from 0.1 mm (Sathe et al. (2010) [10]) to 35 mm (Sathe et al. (2013) [11]), and viscosity of continuous phase. The measured quantities are usually terminal rise velocity, bubble shape and rising path.

Figueroa-Espinoza et al. (2008) [7] studied effect of confinement on bubble motion for Reynolds numbers below 500 with ratio of bubble radius to channel gap from 0 (bubble without confinement) to 0.5 (bubble contacts the channel surface in both sides). They found that ratio between drag coefficient with confinement to that without confinement had a strong dependence on s in the investigated range : $F(s)=1+ks^3$. k is 8 for rectilinear rising bubble with Reynolds number below 70, and is 80 for oscillating bubbles with Reynolds number above 70. Both s and bubble rising path can affect the drag coefficient in confined channel, and affect further bubble rising velocity.

However, in order to disclosure the differences between flow patterns of air-water two phase flow and that of vapor-water two phase flow, comprehensive research of single bubble behavior including bubble shape, bubble trajectory, bubble velocity and bubble wake in narrow rectangular channel is necessary besides earlier studies. In the present research, employing PIV (Particle Image Velocimetry) we studied experimentally single air bubble behavior in rectangular channel of $2\times 60\times 950$ mm^3 with bubble volume equivalent diameter ranging 2.5 mm to 24 mm under inlet average velocities of 0.0-0.2 m/s. In addition, with Level set method based on TransAT, we calculated and discussed the results in comparison with experimental results. All cases were performed at atmospheric pressure and 15^{o}C.

2. EXPERIMENTS

2.1. Experimental facility

Experimental facility consists of three parts: experimental loop, bubble generation system and PIV system. The experimental loop shown schematically in Fig. 1(a) comprises a rectangular test section, an inlet water tank, an outlet water tank, a venturi flowmeter, a preheater, an air compressor and a centrifugal pump. Design pressure of the experimental loop is 1 MPa and the maximum operating temperature is 120^{o}C. The outlet water tank is 6 m from the ground which can produce stable flow velocity up to about 10 m/s. Water from the outlet tank goes through venturi flowmeter then heated by preheater to set temperature. The heated water enters the test section from the bottom and then flows to the inlet water tank. Pump drives water to the outlet tank to recycle the deionized water finally. Design power of the preheater is 89.4 kW. Design mass flow rate of venturi is 0.0027-0.061 kg/s working at atmospheric pressure. The working flow rate of venture flowmeter is 0.006-0.030 kg/s with an accuracy of 0.5%. Head of the centrifugal pump is 24 m with a maximum flow rate of 3.83×10^{-4} m^3/s.

The rectangular test section (Fig. 1(b)) was made up of insulated quartz glasses which can meet the transmittance requirement to obtain clear image. Considering that the bubbles have to move a certain distance before being steady, length of the test section was chosen to be 950 mm. Two pieces of quartz

glass ($950 \times 120 \times 4.5$ mm^3) were fastened by aluminum alloy frame. A resin gasket that can stand 350^{o}C was set between two pieces of quartz glasses to seal up and adjust the gap of the flow duct from 1 mm to 3 mm. In the present paper, only 2 mm gap was studied, and other gap size will be studied further. Cross section of the channel is 60×2 mm^2 with a length of 950 mm. The test section was connected with the loop by two circular tubes.

Table I. Comparison between calculated and experimental terminal velocities

References	Channel geometry (width × length × hight) (mm^3)	Bubble Size (mm)	Varied parameters	Measured quantity
Bohm et al. (2014) [5]	5-7× 160× 1500	3-9	Bubble size, Newtonian or non- Newtonian liquid	Effect of channel space and liquids on bubble rising behaviour
Drews et al.(2010) [6]	3-11× 160× 700	3-24	Bubble size, viscosity	Bubble velocity
Figueroa-Espinoza et al. (2008) [7]	3.6/4.7× 160× 700	< 1.4	Re	Drag coefficients
Maneri and Zuber (1974) [8]	(9.5-1.3)× (63-86)× 914	< 55	Channel inclination, viscosity	Bubble velocity
Roudet et al. (2007) [9]	1× 400× 800	2.6-8.3	Bubble size, channel inclination,	Shape, bubble velocity, oscillation
Sathe et al. (2010) [10]	200× 15× 500	0.1-15	Bubble size, liquid velocity	Comparison between single bubble behaviour and bubble swarms
Sathe et al. (2013) [11]	200× 15× 1000	2-35	Bubble size	Bubble diameter
Vries et al. (2002) [12]	15× 15× 500	0.8-1.8	Bubble size	Effect of wall on bubble rising path

2.2. Measurement technique

PIV was used to restructure the flow field in front of a single gas (vapor) bubble and in the wake. The PIV system used for the determination of the flow field is mainly composed of a pair of high-resolution charge coupled device (CCD) cameras (LaVision FlowMaster3 system) with Nikon lens, a double pulsed Neodymium-doped Yttrium Aluminium Garnet (Nd :YAG) laser and a LaVision's "FlowMaster3" correlator for data processing of PIV images. To simultaneously capture the images of both bubbles and tracer particles, a laser induced fluorescence (LIF) technique was applied. Red fluorescent polymer microspheres with a density of 1000 kg/m^3 and a mean diameter of 8 μm were seeded in the flow. The tracer particles were homogeneously distributed in the whole inlet water tank. A double pulsed laser at 532 nm wavelength was used to illuminate a vertical cross-section of the channel. The observed field is 60×130 mm^2 located at a height of 300 mm above the centerline of the inlet pipe. Bubbles rise at their

terminal velocity within the viewing field. The frame straddling technique was applied to measure the flow field. Two successive exposures of the flow to the laser light sheet were recorded by CCD camera. The time interval was set to be 2.0-4.0 ms depending on different operating conditions of the experiments. The intensity of the laser was 200 mJ/pulse, and the thickness of the laser beam is 1-2 mm. The error of velocity measurement is 1%.

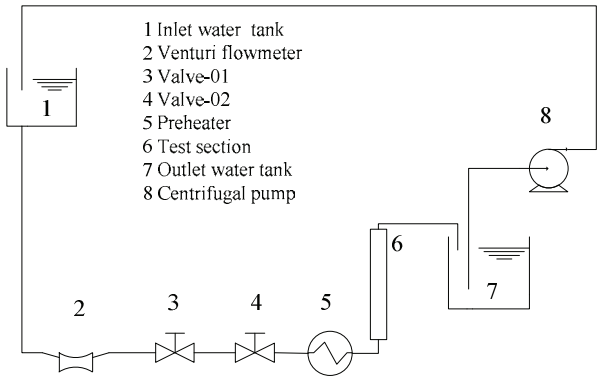

Fig. 1(a). Flow diagram of experimental loop

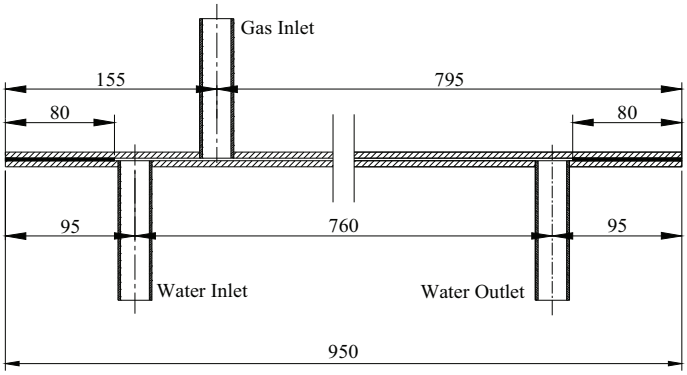

Fig. 1(b). Sectional view of the test section (2 mm gap)

3. NUMERICAL MODEL

3.1. Level Set Method

The Level Set approach (Osher & Sethian(1988)[13]) consists in solving a hyperbolic equation:

$$\frac{\partial \phi}{\partial t} + u_j \nabla \phi = 0 \tag{1}$$

to track the interface on a fixed Eulerian grid, where $\phi(x,t)$ is a smooth signed-distance function referring to the shortest distance to the front. Negative values correspond to one of the fluids and positive values to the other. The exact location of the interface corresponds to the zero level of ϕ , so we have,

$$\phi(x,t)=\begin{cases}>0, & x\in \textit{Liquid}\\ =0, & x\in \textit{Interface}\\ <0, & x\in \textit{gas}\end{cases} \tag{2}$$

To update material properties like density, viscosity and thermal conductivity, a Heaviside function H(ϕ) is introduced,

$$\rho=\rho_l H(\phi)+\rho_g(1-H(\phi)) \tag{3}$$

$$\mu=\mu_l H(\phi)+\mu_g(1-H(\phi)) \tag{4}$$

and Heaviside function H(ϕ) is defined as:

$$H(\phi)=\begin{cases}0, & \phi<0\\ 1, & \phi\geq 0\end{cases} \tag{5}$$

A modified Heaviside function denoted by $\overline{H}(\phi)$ is employed to smooth the physical properties across an interface with a thickness of 2δ ,

$$\rho(\phi,t)=\sum_k \rho_k \overline{H}(\phi) \tag{6}$$

$$\overline{H}(\phi)=\tanh(2\phi/\delta) \tag{7}$$

The same modified Heaviside function is concurrently employed to determine the surface tension.

3.2. Equations of two-phase flow

After defining the Level Set function ϕ , the unmixed liquid and gas phase divided by phase interface can be considered as a mixture, and can be described by the continuity equation and momentum equation as follows,

$$\frac{\partial u_j}{\partial x_i}=0 \tag{8}$$

$$\frac{\partial(\rho u_j)}{\partial t}+\frac{\partial(\rho u_i u_j)}{\partial x_j}=\frac{\partial}{\partial x_j}(-p\delta_{ij}+\sigma_{ij})+\rho g_i+\rho\gamma k\delta^I(\phi)n_i \tag{9}$$

where γ is the surface tension coefficient, k is the interface curvature, n_i is the normal vector to the interface, δ^I is a smoothed Dirac delta function centered at the interface, material properties are updated using equation (3),(4) and (6).

3.3. Numerical solving method

Finite volume method was used to discrete governing equations in the non-staggered grid. Velocity, density, pressure and Level Set function are all defined at center point of each grid. We used Runge-Kutta with 2nd order precision and 3rd order upwind scheme to solve the Level Set equation. Main flow field of gas-liquid two phase flow was calculated through ALE (Arbitrary Lagrangian Eulerian) algorithm. Time step was adaptive with a initial value of 0.001s, and the mesh was hexahedron with volume of 0.5 mm^3 determined by grid analysis.

As numerical errors cause the contours of the Level Set field to deform as the phase moves, a re-distancing algorithm was required to regularize the function and conserve the volume or mass of the

particle: advecting the initial distance function $\phi(x, 0)$ will not be maintained as such. An extra re-distancing algorithm preserving $|\nabla\phi| = 1$ around the zero level of ϕ is required [14].

4. RESULTS AND DISCUSSIONS

4.1. Terminal Rising Velocity

To verify the validation of test method and data attained, we compared the experimental data with classical results of Clift et al. (1978) [4] in unconfined water and Bohm et al.(2014) [5] in narrow rectangular channel with gap of 5 mm. Fig. 2 shows relative terminal velocity of single bubbles. Relative terminal velocity was calculated by absolute rising velocity minusing the inlet average fluid velocity.

The standard deviation of each data point is too small to be visible in the diagram. For all parameter combinations in pure water, increasing the bubble size (in the range investigated here) leads to bubble rising velocity first increasing, then decreasing, and increasing finally due to the beginning of bubble deformation. This is the intrinsic property for single bubble rising in pure water [4]. The transition diameter was 1.4 mm and 6 mm separately. Experimental data present and that of Bohm et al.(2014) [5] are all consistent with the rule. Specific diameter and rising velocity varied among the three set data, which was mainly attributed to wall effect caused by narrow gap [7].

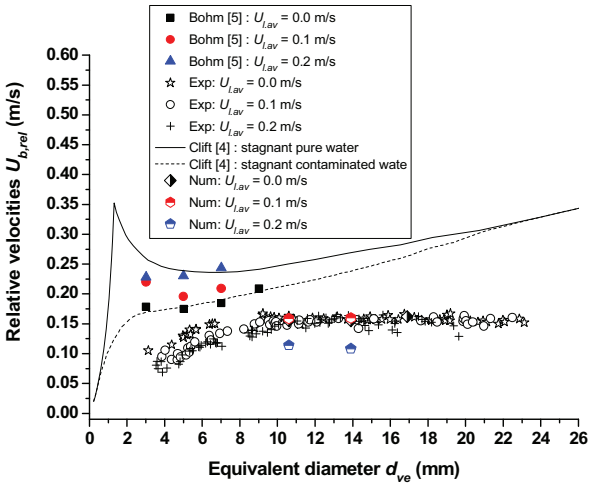

Fig. 2. Relative terminal velocity of single bubbles in vertical narrow rectangular channel(Exp means "Experimental data", Num means "Numerical data")

A clear distinction between three inlet average velocity levels is shown. When bubble diameter was less than 10 mm, its relative terminal velocity decreased as inlet average fluid velocity increased, which are opposite with that of Bohm's result. Our test section was $2 \times 60 \times 950$ mm^3. Test section of Bohm was $5 \times 160 \times 1500$ mm^3 supplying more space for bubble rising, which might changed velocity profile across the channel and further affected bubble relative rising velocity. The distinct phenomenon needs to study further. When bubble diameter was beyond 10 mm, experimental data showed that the inlet average fluid velocity did not strongly affect the bubble relative velocity. By contrary, numerical results showed that bubble relative terminal velocity decreased obviously as inlet average fluid velocity increased. Numerical

data are consistent with result of OZDEMIR (2005)[16] whose test section was 2.1 × 66.5 × 607 mm^3 similar to test section in present research. If bubble rising velocity changed, it might attribute to bubble shape or bubble trajectory changing. Bubble shape and trajectory are all influenced by the flow field in the wake. From Fig. 2 and Fig. 3, we can clearly see that inlet average fluid velocity affected bubble shape and almost had no effect on bubble trajectory. Bubble deformation was symmetric which indicated that force acted on the bubble were symmetric. Because of this reason, the bubble trajectory maintained linear. Large bubble surface area corresponding to large bubble deformation under larger inlet average fluid velocity caused more friction or shape drag. On the basis of the increased drag, the bubble relative rising velocity reduced. In summary, the superimposed liquid velocity will reduce relative velocity of bubble rising in water in narrow rectangular channel.

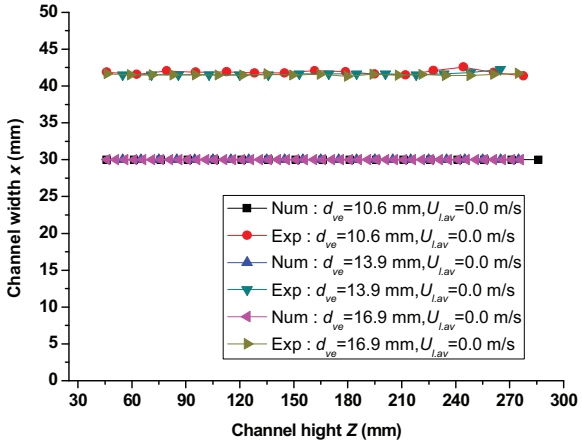

Fig. 3. Bubble trajectory under different inlet average fluid velocities

4.2. Bubble shape

Many investigators have studied bubble shape [16]. They used static dimensionless numbers Eo (or Bo) and Mo or dynamic dimensionless number Re and We to express the bubble aspect ratio. In addition, dimensionless number Ta containing both static and dynamic parameters was also used. However, general correlation cannot reveal the detailed deformation such as a dimple on the aft end of bubble [16]. Here we studied numerically and experimentally effect of inlet average fluid velocity on bubble shape (Fig. 4). Calculated and experimental bubble shape was similar. Both numerical and experimental results showed that the superimposed liquid velocity caused formation of dimple on the aft end of bubble. The larger the superimposed liquid velocity, the deeper the dimple. Bubble deformation is governed by flow field around the bubble. Fig. 4 shows that fluid falling along both sides of bubble first flows downward, then becomes stagnant and finally flows upward as the inlet average fluid velocity increasing. Their interaction on the bubble was always symmetric. Fluid below bubble flows faster and faster as the inlet average fluid velocity increases. At the case with inlet average fluid velocity of 0.1 m/s, 0.1 m/s was less than the bubble rising velocity in stagnant water. However, due to the fluid falling down from bubble sides, the fluid velocity below bubble was a litter higher than bubble rising in stagnant water, which caused the bubble deforming slightly. Stronger impact force acted on the bubble bottom surface deforms the bubble more obviously with increasing inlet average velocity.

4.3. Wake characteristics

4.3.1 Wake structure

Wake structure is of great significance for bubble interaction. To simplify, we first studied wake of single bubble. Influence of inlet average fluid velocity on bubble wake was listed in Fig. 5. Experimental image of wake were obtained by PIV. Numerical wake fields were reconstructed by Praview with arrow indicating fluid flow direction. Numerical wake fields were all similar to that of experimental shot. In stagnant water, two long symmetric vortex were in the wake. Symmetric vortexes in the wake were longer for large bubbles. Influence area and structure of wake is governed by velocity of falling liquid film through gap between bubble and channel wall. Greater liquid velocity from narrower gap when bubble is larger forms longer vortex and more. When the falling liquid film caused by bubble rising meets the upward flowing inlet fluid, the combined velocity becomes smaller. Falling liquid film with lower speed contributed to shorter vortex and less influence area of wake. When the inlet average fluid velocity increases to certain extent, there will no falling liquid on both sides of rising bubble and no disturbance in the wake as well (Fig.4 (a3) and Fig. 4(b3)).

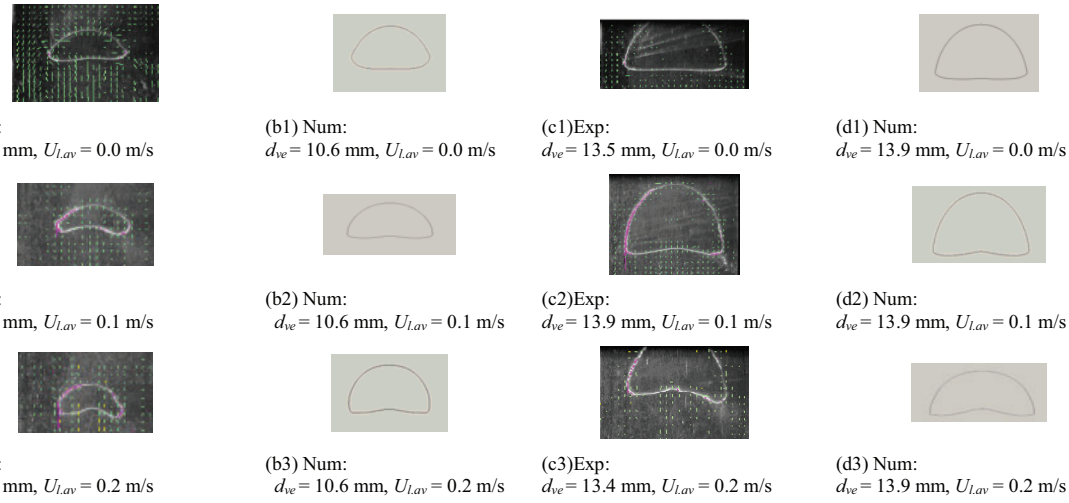

(a1)Exp: d_{ve} = 9.8 mm, $U_{l.av}$ = 0.0 m/s
(b1) Num: d_{ve} = 10.6 mm, $U_{l.av}$ = 0.0 m/s
(c1)Exp: d_{ve} = 13.5 mm, $U_{l.av}$ = 0.0 m/s
(d1) Num: d_{ve} = 13.9 mm, $U_{l.av}$ = 0.0 m/s
(a2)Exp: d_{ve} = 9.7 mm, $U_{l.av}$ = 0.1 m/s
(b2) Num: d_{ve} = 10.6 mm, $U_{l.av}$ = 0.1 m/s
(c2)Exp: d_{ve} = 13.9 mm, $U_{l.av}$ = 0.1 m/s
(d2) Num: d_{ve} = 13.9 mm, $U_{l.av}$ = 0.1 m/s
(a3)Exp: d_{ve} = 9.6 mm, $U_{l.av}$ = 0.2 m/s
(b3) Num: d_{ve} = 10.6 mm, $U_{l.av}$ = 0.2 m/s
(c3)Exp: d_{ve} = 13.4 mm, $U_{l.av}$ = 0.2 m/s
(d3) Num: d_{ve} = 13.9 mm, $U_{l.av}$ = 0.2 m/s

Fig. 4. Bubble shape under different inlet average fluid velocities

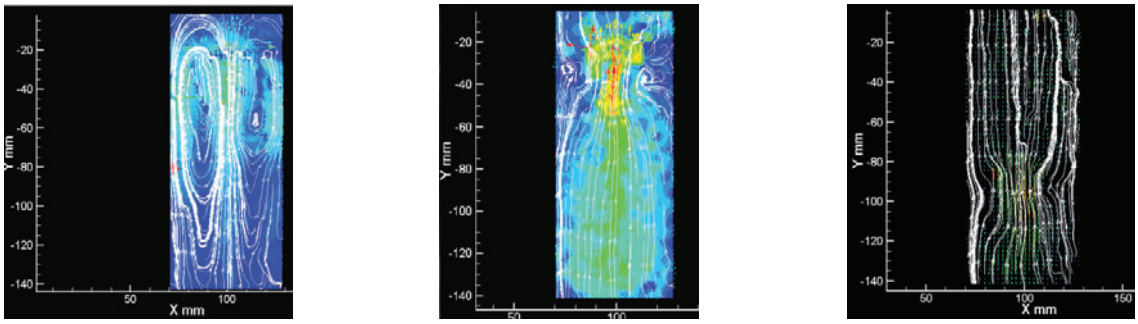

(a1) Exp: d_{ve} = 9.8 mm, $U_{l.av}$ = 0.0 m/s
(a2) Exp: d_{ve} = 9.7 mm, $U_{l.av}$ = 0.1 m/s
(a3) Exp: d_{ve} = 9.6 mm, $U_{l.av}$ = 0.2 m/s

(b1) Num: d_{ve} = 10.6 mm, $U_{l.av}$ = 0.0 m/s

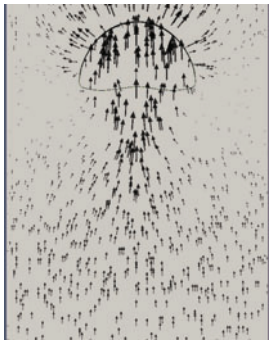

(b2) Num: d_{ve} = 10.6 mm, $U_{l.av}$ = 0.1 m/s

(b3) Num: d_{ve} = 10.6 mm, $U_{l.av}$ = 0.2 m/s

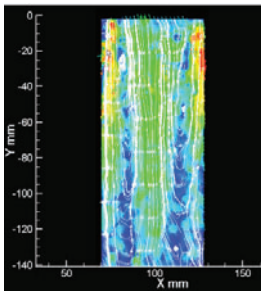

(c1) Exp: d_{ve} = 13.5 mm, $U_{l.av}$ = 0.0 m/s

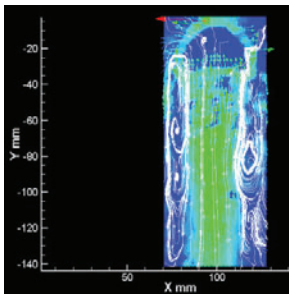

(c2) Exp: d_{ve} = 13.9 mm, $U_{l.av}$ = 0.1 m/s

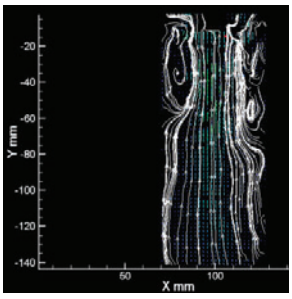

(c3) Exp: d_{ve} = 13.4 mm, $U_{l.av}$ = 0.2 m/s

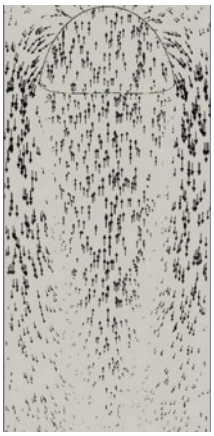

(d1) Num: d_{ve} = 13.9 mm, $U_{l.av}$ = 0.0 m/s

(b2) Num: d_{ve} = 13.9 mm, $U_{l.av}$ = 0.1 m/s

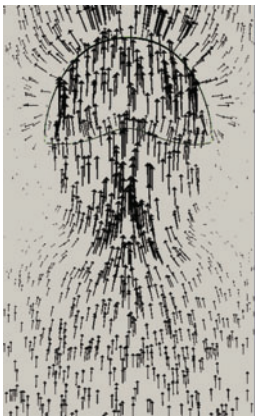

(b3) Num: d_{ve} = 13.9 mm, $U_{l.av}$ = 0.2 m/s

Fig. 5. Bubble wake structure under different inlet average fluid velocities

4.3.2 Velocity profiles in the Wake

From the wake structure analysis, we know that velocity profile around bubble was also changed by the inlet average fluid velocity. Here we discussed calculated flow field in front of and behind single bubbles in stagnant water and flowing water (Fig. 6-Fig. 9). Fig. 6 and Fig. 7 correspond to the cross section with maximum velocity in Fig .8 and Fig. 9 separately. Fig. 6 shows horizontal distributions of absolute velocity at the tip of single bubble. Inlet average fluid velocity changed the velocity profile ahead of bubble: Maximum velocity was not at the tip as in stagnant water but moved to two sides. As the Inlet average fluid velocity increased, velocity of fluid on both sides changed from flowing downward to

upward, which can explain the weak disturbance (Fig. 6). Curve shape of velocity profiles behind the bubble were consistent with bubble shape (Fig. 7) which showed that fluid at the bubble dimple has the maximum velocity of the whole cross section. For longitudinal distributions of absolute velocity in the channel center ahead of bubble, Fig. 8 shows that position reaching stable velocity is about $0.75W$ from the bubble tip and the position is not affected by the inlet average fluid velocity. In contrast, position with maximum velocity in the wake moved to the bubble bottom as the Inlet average fluid velocity increased (Fig. 9) which might attribute to bubble shape with dimple.

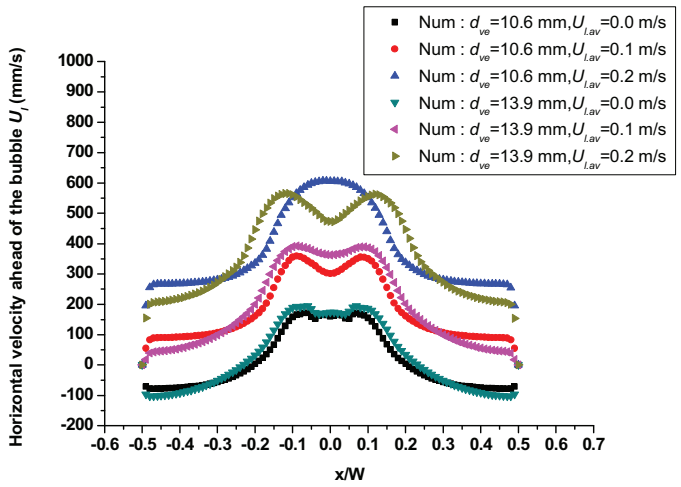

Fig. 6. Horizontal distributions of absolute velocity ahead of single bubble

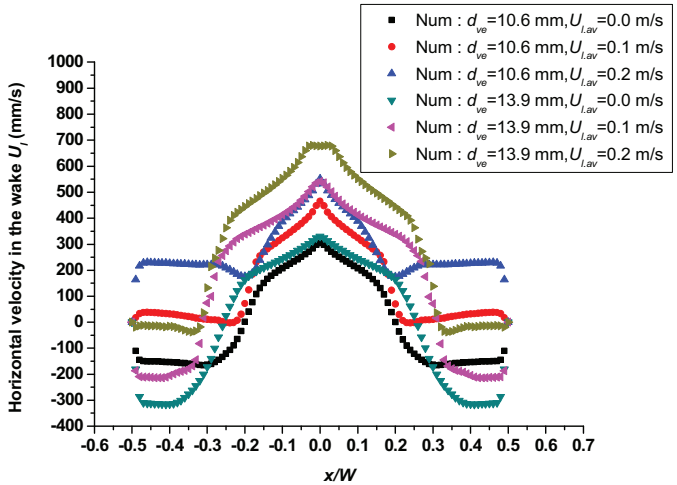

Fig. 7. Horizontal distributions of absolute velocity behind single bubble

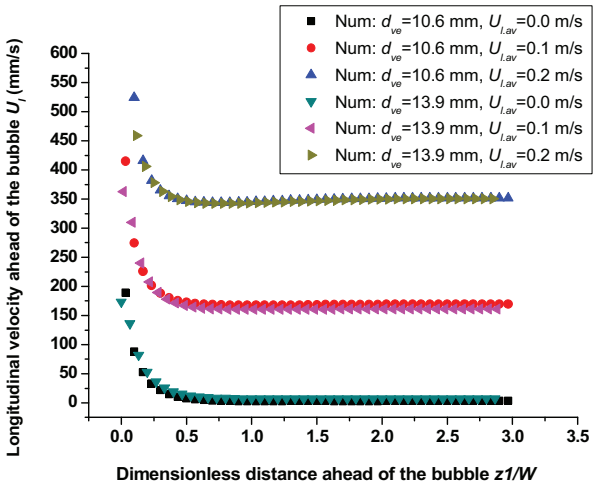

Fig. 8. Longitudinal distributions of absolute velocity ahead of single bubble

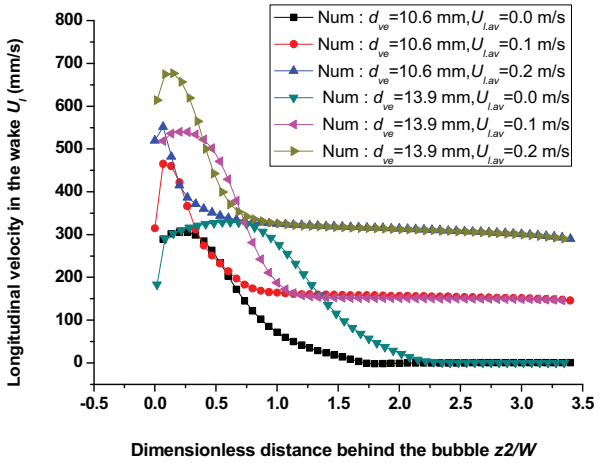

Fig. 9. Longitudinal distributions of absolute velocity behind single bubble

5. CONCLUSIONS

In the present paper, we numerically and experimentally study the motion characteristics of single air bubble rising in a vertical narrow rectangular channel, and analyze effects of inlet average fluid velocity on terminal rising velocity, bubble shape, wake structure and velocity profiles. Air bubbles were produced by injecting air into the test section of 60 × 2 × 950 mm^3, and bubbles with diameter of 2.0-24.5 mm rising through water with inlet average fluid velocities 0.0-0.2 m/s were examined by PIV (Particle Image Velocimetry). We did the numerical analysis employing Level Set method based on TransAT software. Conclusions can be drawn as follows.

(1) Inlet average fluid velocity can reduce relative rising velocity of single bubble in vertical narrow rectangular channel. Increasing inlet average fluid velocity led to deeper dimple on bubble bottom surface which might contribute to lower relative rising velocity of bubble. Linear bubble trajectory of larger bubbles was not affected by inlet average fluid velocity.

(2) Influence area and structure of wake is governed by velocity of falling liquid film through gap

between bubble and channel wall. Greater liquid velocity from narrower gap when bubbles are larger forms longer vortex and more influence area. Falling liquid film with lower speed led to shorter vortex and less influence area of wake. Increasing inlet average fluid velocity caused less disturbances in the wake.

(3) Position achieved stable velocity ahead of bubble was about 0.75 D from bubble tip and not affected by inlet average fluid velocity. But Position with maximum velocity in the wake moved to bubble bottom as inlet average fluid velocity increased.

(4) Numerical results by Level-set model predicted these experimental results rather well. The comparisons were presented on the basis of detailed bubble behavior.

NOMENCLATURE

A_b	bubble's projection on the wide side of the narrow rectangular channel, m^2
d_{ve}	volume equivalent diameter of bubbles, m; $(\sqrt[3]{6A_b\delta/\pi})$, for bubbles greater than the channel gap
g	gravity acceleration, m/s^2
s	dimensionless diameter of bubbles; (d_{ve}/δ)
$U_{b,t}$	terminal velocity of the rising bubble, m/s
$U_{b,rel}$	relative velocity of the bubble, m/s, $U_{b,rel} = U_{b,t} - U_{l,av}$
$U_{l,z}$	transient and local velocity in the flow field, m/s
$U_{l,av}$	inlet average fluid velocity of water, m/s
W	width of the rectangular channel, m
x	direction is along the wide side of channel, the left edge is $x = 0$ m; and the right edge is $x = 0.6$ m
$z1$	distance ahead of the bubble tip, m
$z2$	distance behind the bubble tail, m

Greek Letters

δ	gap of the rectangular channel, m
μ_l	dynamic viscosity of water, Pa s
π	circumference ratio, 3.1416

ρ_l density of water, kg/m^3

σ_l surface tension of water, N/m

Non-dimensional Numbers

Eo Etvos number; $\left(\frac{\rho_l g d_{ve}^2}{\sigma_l}\right)$

Bo Bond number; $\left(\frac{\rho_l g (0.5 d_{ve})^2}{\sigma_l}\right)$

Mo Morton number; $\left(\frac{g \mu_l^4}{\rho_l \sigma_l^3}\right)$

Re Reynolds number; $\left(\frac{\rho_l U_{l,av} d_{ve}}{\mu_l}\right)$

We Weber number; $\left(\frac{\rho_l^2 g d_{ve}^3}{\mu_l^2}\right)$

Ta Tadaki number; $Re_p\, Mo^{0.23}$

Subscripts or superscripts

av average

b bubble

l liquid

rel relative

t terminal

ve volume equivalent

Abbreviations and acronyms widely used in the text and list of references

CCD Charge Coupled Device

LIF Laser Induced Fluorescence

Nd:YAG Neodymium-doped Yttrium Aluminium Garnet

PIV Particle Image Velocimetry

Exp	Experimental
Num	Numerical

ACKNOWLEDGMENTS

Supports of National Natural Science Foundation of China through grant No. 51176176 and National Science Foundation for Distinguished Young Scholars of China through grant No. 11325526 are gratefully acknowledged.

REFERENCES

1. J. Wang, Y. Huang, Y. Wang, "Visualized experimental observation on flow patterns in a single-side heated narrow rectangular Channel," *Nucl. Power .Eng*. **31**(6), pp. 80-92 (2010) (In Chinese).
2. Y. Wang, B. Chen, Y. Huang, J. Wang, "Experimental Research on evolvement of Density Wave Oscillation in Parallel Narrow Rectangular Channels," *Nucl. Power. Eng*. **32**(5), pp. 75-79 (2011) (In Chinese).
3. J. Huang, Y. Huang, J. Ma, Y. Wang, Q. Wang, "Visual study on bubbles by longitudinal vortex in narrow channel," *Chem. Eng (China)*. **40**(7), pp. 46-51 (2012) (In Chinese).
4. R. Clift, J. R. Grace, M. E. Weber, *Bubbles, Drops, Particles,* Chapter 9, Academic Press, London and England (1978).
5. L. Bohm, T. Kurita, "Rising behaviour of single bubbles in narrow rectangular channels in Newtonian and non-Newtonian liquids," *Int. J. Multiphase Flow.* **65**, pp. 11-23 (2014).
6. A. Drews, H. Prieske, E. L. Meyer, G. Senger, M. Kraume, "Advantageous and detrimental effects of air sparging in membrane filtration: bubble movement,exerted shear and particle classification," *Desalination.* **250** (3), pp. 1083–1086 (2010).
7. B. Figueroa-Espinoza, R. Zenit, D. Legendre, "The effect of confinement on the motion of a single clean bubble," *J. Fluid Mech.* **616**, pp**.** 419-443 (2008).
8. C. Maneri, N. Zuber, "An experimental study of plane bubbles rising at inclination," *Int. J. Multiphase Flow*. **1** (5), pp. 623–645 (1974).
9. M. Roudet, V. Roig, A. M. Billet, F. Risso, "Paths and shapes of two dimensional rising bubbles at high-Reynolds number," *Proceedings of the ICMF, 6th International Conference on Multiphase Flow*, Allemagne, July 9 (2007).
10. M. J. Sathe, I. H. Thaker, T. E. Strand, J. B. Joshi, "Advanced PIV/LIF and shadowgraphy system to visualize flow structure in two-phase bubbly flows," *Chem. Eng. Sci*. **65** (8), pp. 2431–2442 (2010).
11. M. J. Sathe, J. B. Joshi, G. Evans, "Characterization of turbulence in rectangular bubble column," *Chem. Eng. Sci*. **100**, pp. 52–68 (2013).
12. A.W.G. de Vries, A. Biesheuvel, L. Wijngaardenvan, "Notes on the path and wake of a gas bubble rising in pure water," *Int. J. Multiphase Flow*. **28** (11), pp. 1823–1835 (2002).
13. S. Osher, J. A. Sethian, "Fronts propagating with curvature-dependent speed: Algorithms based on hamilton-jacobi formulations," *J. Comp. Phys*. **79**, pp.12-49 (1988).
14. M. Sussman, P. mereka, S. Osher, "A level set approach for computing solutions to incompressible two-phase flow," *J. Comp. Phys*. **114**, pp. 146-159 (1994).
15. S. OZDEMIR. *Investigation of air bubble motion in water through a vertical narrow rectangular channel by using image processing techniques*. PhD Thesis , Middle East Technical University (2005).
16. E. Loth, "Quasi-steady shape and drag of deformable bubbles and drops," *Int. J. Multiphase Flow.* **34**, pp. 523–546 (2008).